EUROPEAN LABORATORY FOR PARTICLE PHYSICS

CERN/TIS-RP/95-17/CF

REFLECTIONS ON A FLAT WALL

Graham R. Stevenson and Mika Huhtinen

Abstract

This paper describes an investigation into whether estimates of attenuation in the flat side-walls of the tunnel for the LHC main ring can be based on a simple point-source/line-of-sight model. Having seen the limitations of such a model, an alternative is proposed where the main radiation source is not the initial object struck by the beam but the plane source provided by the first interactions of secondaries from the target in the shield-wall. This is shown to have a closer relation to reality than the point-source/line-of-sight model.

To be presented at the
Second Workshop on Simulating Accelerator Radiation Environments,
CERN, Geneva, Switzerland, 9–11 October 1995

CERN, Geneva, Switzerland
4th October 1995

Reflections on a Flat Wall

Graham R. Stevenson and Mika Huhtinen
CERN, 1211 Geneva 23, Switzerland

Abstract

This paper describes an investigation into whether estimates of attenuation in the flat side-walls of the tunnel for the LHC main ring can be based on a simple point-source/line-of-sight model. Having seen the limitations of such a model, an alternative is proposed where the main radiation source is not the initial object struck by the beam but the plane source provided by the first interactions of secondaries from the target in the shield-wall. This is shown to have a closer relation to reality than the point-source/line-of-sight model.

1 INTRODUCTION

Until recently, most simulation studies for shield design were usually performed in geometries having cylindrical symmetry. The powerful biasing features introduced into the latest versions of the FLUKA code [1, 2] together with the CPU power now available in work-stations such as the IBM RS6000 machines have recently made possible the consideration of deep penetration simulations in realistic non-symmetric geometries. This report contains some philosophical reflections which were developed in the course of simulating the effect of beam losses in a magnet string in a region of the tunnel of the LHC main ring where the shield wall on one side of the accelerator is a long flat wall [3]. The data obtained in this work was used to test the validity of empirical shielding formulae.

2 LATERAL SHIELDING OF THE LHC MAIN RING

The geometrical situation is shown in Figure 1. The coordinate system was defined so that the positive z-axis coincided with the beam direction. The positive y-axis pointed upwards and the positive x-axis pointed towards the flat wall. The beam axis defined the origin in the xy-plane . In Figure 1 the beam direction is perpendicular to the page coming towards the reader. For this specific problem, the magnet was modeled as a 35 m long solid iron cylinder of 20 cm radius. The 7 TeV protons entered the system at the centre of this cylinder at $z = 6$ m. The concrete floor was 80 cm below the beam axis and was assumed to have a thickness of 20 cm. The curved part of the wall was taken to be part of a concrete cylinder of 6.75 m inner radius and 20 cm thickness. The centre of this cylinder did not coincide with the beam axis, but was located at $(x, y) = (4.45\text{ m}, 0.35\text{ m})$. The flat part of the concrete wall started at $x = 2.9$ m and had a thickness of 3 m.

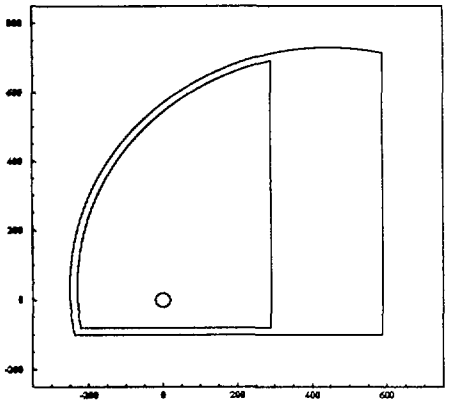

Figure 1: Cut in the xy-plane through the flat wall geometry used in the simulations. The iron target is centred at $x = y = 0$ and the walls are concrete. Dimensions are given in cm.

The floor and curved wall were not of prime importance for the present study of transmission in the flat wall since they only contributed back-scattered particles, Therefore they were made only 20 cm thick and a Russian Roulette biasing factor was applied for particles entering them: on average only one out of two was allowed to survive the entry into the curved wall and floor. This biasing strategy had the additional beneficial effect that back-scattered particle histories were on average split into two. In the flat wall section, region-importance biasing was used with a splitting factor of 1.3 every 20 cm in depth. Since the attenuation length in concrete is of the order of 50 cm, the attenuation factor over 20 cm is 0.67, which would suggest that a splitting factor of 1.5 would be required in order to achieve a linear behaviour in the number of histories followed as a function of depth in the wall. However, it has been found that it is generally safer to use too small rather than too large a factor, since artificial correlations introduced by the splitting are better suppressed and the cost in CPU time is in general acceptable. Too large a splitting factor can in fact result in a significant waste of CPU time and correlations often dominate: convergence might appear to be excellent but it is not necessarily to the correct value. The factor of 1.3 has been shown to maintain an excellent behaviour up to penetration depths of several metres in concrete [4].

Since biasing destroys the possibility of estimating errors in a single run, the problem was split into seven separate sets, each of 1000 primary 7 TeV protons.

In Reference [4] it was shown that star densities (the den-

sity of inelastic interactions having hadron primaries with energies greater than 50 MeV) can be used to obtain doses in good agreement with those obtained from particle fluxes. Since the scoring of star densities allows one to neglect both the electromagnetic cascade and low-energy neutrons, it is a significantly faster method than performing fluence to dose conversion on all components of the hadronic and electromagnetic cascade. The results presented in this report are obtained from star densities with the standard conversion factor of 1 star/cm^3 in concrete being equivalent to 4.5×10^{-8} Sv [5].

A Cartesian xyz-binning was used in the flat-wall with a granularity of $20 \times 50 \times 50$ cm^3. Starting from y=–80 cm one can fit 15 bins into the flat part of the wall, so the binning ended at y=6.7 m.

In addition to the long target which extended through the whole geometry, a second situation was considered where the target length was only 2 m, starting at z=6 m.

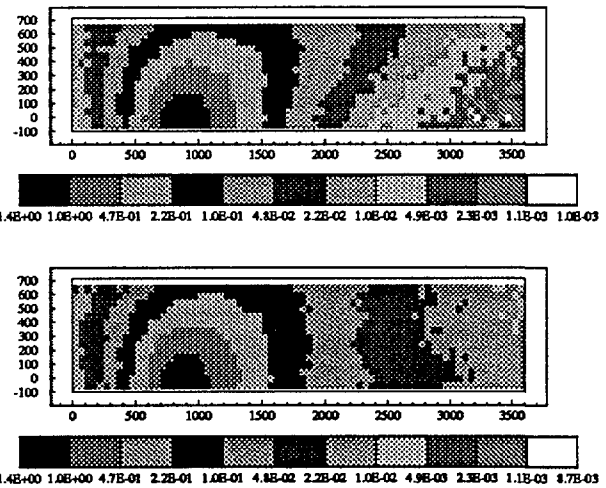

Figure 2: Doses in pSv/proton averaged over the first 20 cm depth of the inner surface of the flat wall. The upper figure is for the 35 m long magnet and the lower for a magnet 2 m in length.

Contour plots of the doses in pSv/proton averaged over the first 20 cm depth of the inner surface of the wall are given in Figure 2. The contours for the long target show that the dose increases with vertical distance from the beam axis at longitudinal distances greater than 10 m downstream of the beam-entry point, which is contrary to a normal intuitive expectation. The contours for the shorter target, however, show the expected regular decrease of dose with vertical distance from the beam axis for all distances downstream of the point of entry of the beam into the target. The increase in dose with vertical distance is thus linked with attenuation in the long iron target and will be investigated further in the following section.

3 POINT-SOURCE/LINE-OF-SIGHT MODELS

3.1 The Models

Two assumptions are often made in shielding calculations. The first is that the source can be approximated by a point source *i.e.* it is localized in a geometrical region which is small in size compared with the other dimensions of the shielding situation. This means that the inverse square law of geometrical dilution will hold.

The second is that the dose, D, as a function of position can be described in terms of the relative co-ordinates of the point source, S, and the point of interest, P (see Figure 3) and that there are no contributions from any other secondary sources. If S is assumed to be at the origin of the co-ordinate system then the dose $D(x, y, z)$ at P which is at a distance R from P and which is at a radial distance off-axis, r, and a longitudinal depth, z, can be described:

$$D(x, y, z) = D(\zeta, \theta), \qquad (1)$$

where ζ is the line-of-sight distance in the shield of the vector joining S to P and $\theta = \arctan(r/z)$ is the polar angle of this vector with respect to the beam axis.

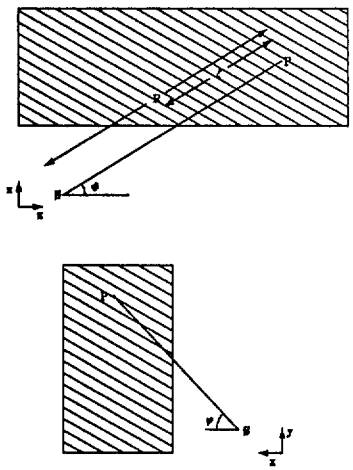

Figure 3: Sketch of the geometry used in the point-source/line-of-sight calculations for an iron cylinder close to a flat shield wall.

Equation (1) represents a pure point-source/line-of-sight model where the radiation field at P is affected only by particles traveling along the vector linking S to P and not from any other point.

The function D can be separated into two other functions: $Z(\zeta, \theta)$ which is a build-up/attenuation function and $\Theta(\theta)$ which is the particle source term as a function of polar angle.

$$D(\zeta, \theta) = Z(\zeta, \theta)\Theta(\theta)/R^2, \qquad (2)$$

The function $Z(\zeta, \theta)$ need not have *a priori* any particular functional form and could have a build-up as well as an attenuation component.

The Moyer Model [5] is one version of a point-source/line-of-sight model which is used for estimating

the shielding required for high-energy proton accelerators. In this model the function $Z(\zeta, \theta)$ does not depend on the polar angle θ and is a pure exponential absorption term of the form $Z(\zeta) = \exp(-\zeta/\lambda)$, where λ is an effective mean free path which is independent of particle type and energy. The angular dependence $\Theta(\theta)$ includes any build-up effect along the line-of-sight and is approximated by a function of the form $\exp(-\beta\theta)$, where β is ≈ 2.3 radians^{-1}. The dose at the point P according to the Moyer model is then:

$$D = D_0 \times \exp(-\beta\theta)\exp(-\zeta/\lambda)/R^2, \qquad (3)$$

where D_0 is a constant which depends on the energy of the incident protons.

3.2 *An Inspection on the Surface*

The dose contours in a flat wall at a depth of 1 cm into the wall were determined using the point-source/line-of-sight model described in the previous section for an isotropic source ($\beta = 0$) and a Moyer-type source ($\beta = 2.3$ radians^{-1}) at the centre of an infinitely long iron cylinder of 20 cm radius whose axis is 2 m laterally away from the wall. The contours for this situation, which are illustrated in Figures 4 and 5, are normalized to the dose at the same depth, 1 m downstream of the target in the $y = 0$ plane. The dose at this point is close to the maximum value. λ in the wall is assumed here to be 50 cm which is approximately the value for high-energy proton induced cascades in concrete. The λ for iron is assumed to be 20 cm.

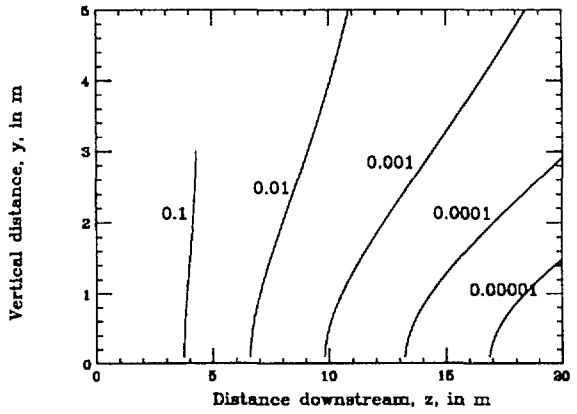

Figure 4: Isodose curves close to the inner surface of a flat wall at a depth of 1 cm for an isotropic source inside an infinitely long iron cylinder of radius 20 cm.

The contours in Figures 4 and 5 show that the dose increases with vertical distance from the beam axis at longitudinal distances downstream greater than about 15 m in the same way as that observed in the FLUKA simulations. This occurs for both the isotropic source and the Moyer-like source. The unexpected shape of the contours is in fact due to attenuation in the long cylinder of iron which "shadows" the wall at small values of θ.

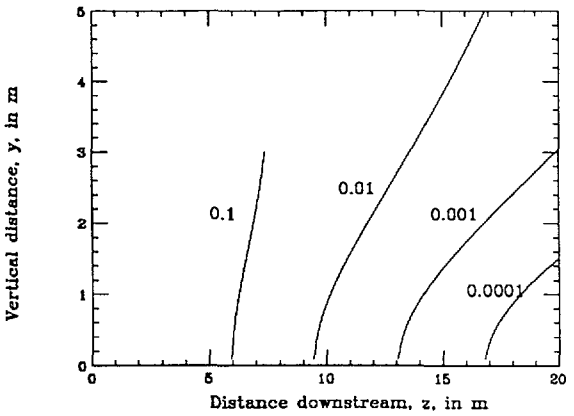

Figure 5: Isodose curves close to the inner surface of a flat wall at a depth of 1 cm for a Moyer-type source with $\beta = 2.3$ radians^{-1} inside an infinitely long iron cylinder of radius 20 cm.

3.3 *Testing in Depth*

The results of the FLUKA simulation for the flat wall provide good data for a more detailed testing of the validity of the line-of-sight models. A first analysis was made for the runs where the protons impinged on the infinitely long iron cylinder of 20 cm radius. For several values of the angle to the proton beam, θ, it was possible to look at the value of the dose equivalent as a function of distance along the line-of-sight and as a function of the azimuthal angle, ϕ (this is the angle which the line-of-sight vector when projected on to the $z = 0$ plane makes with the x-axis.) The point source was assumed to be at a distance of 50 cm downstream of the point of impact of the protons, In Figure 6 the values of dose equivalent multiplied by the square of the distance to the source are shown as a function of line-of-sight depth in the shield for values of θ ranging from 20 to 80°.

It will be seen that the points taken from different lines corresponding to different azimuthal angles all follow a simple exponential dependence on depth, suggesting that a Moyer-type model could be appropriate. However the effective mean free path increases as the polar angle decreases, and this contradicts one of the tenets of the Moyer model *viz.* that λ should be independent of angle. The effective mean free path corresponds to the value expected, slightly less than 50 cm, only at $\theta = 80°$.

The increase of λ with decreasing θ is even more marked for a second series of runs made with a target cylinder of only 2 cm radius (see Figure 7). This suggests that the situation may correspond more to one where secondary interactions along the inner layer of the shield wall are acting as the effective source, rather than there being a single point-like source in the target.

Even though the studies described in this paper were directed towards shielding evaluations at proton energies of 7 TeV, simulations were also performed for the 35 m long target at proton energies of 10 GeV, 100 GeV and 1 TeV. in order to determine whether the variation of the effective mean free path found were unique to the high-multiplicity

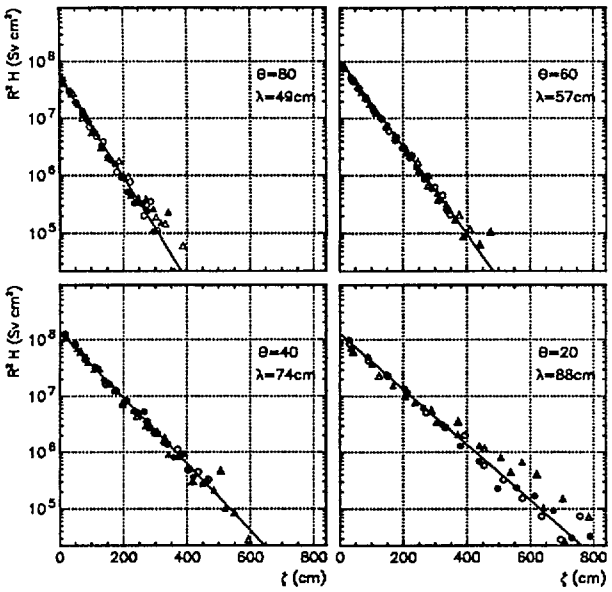

Figure 6: Attenuation along the line of sight for various polar angles, θ, for a 20 cm radial thickness target. Closed circles – $\phi = 0°$, Open circles – $\phi = 15°$, Closed triangles – $\phi = 30°$, Open triangles – $\phi = 45°$.

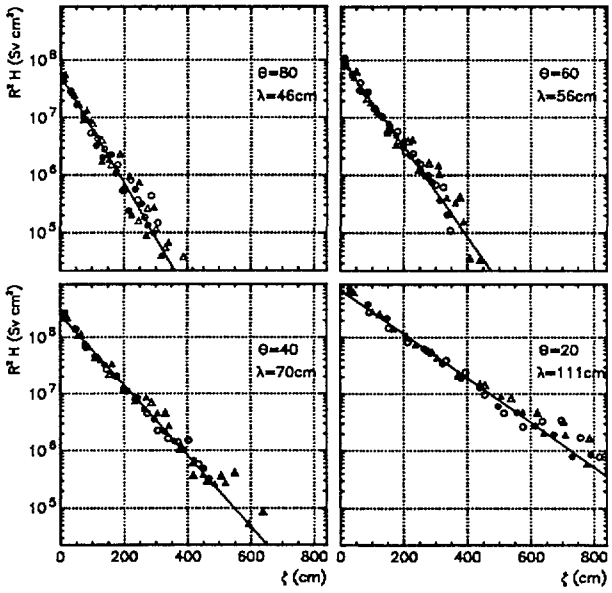

Figure 7: Attenuation along the line of sight for various polar angles, θ, for a 2 cm radial thickness target. Closed circles – $\phi = 0°$, Open circles – $\phi = 15°$, Closed triangles – $\phi = 30°$, Open triangles – $\phi = 45°$.

cascades initiated by 7 TeV protons. Values of the effective mean free path for the various proton energies at the four values of polar angle investigated (averaged over all azimuthal angles) are given in Table 3.3. The values for a given θ for the 20 cm radius target are essentially the same given the fitting error and the slight systematic spread of values for the different azimuthal angles ϕ, which can be seen in Figures 6 and 7. The increase of λ with decreasing θ is not a function of proton energy and is therefore something more fundamentally connected with the assumptions made in the point-source/line-of-sight model.

Table 1: Effective mean free paths (cm) in the concrete wall for different values of θ at various proton energies

Proton Energy	$\theta = 80°$	$\theta = 60°$	$\theta = 40°$	$\theta = 20°$
r = 20 cm				
7 TeV	49	57	74	88
1 TeV	51	57	69	91
100 GeV	52	59	72	99
10 GeV	50	57	73	98
r = 2 cm				
7 TeV	46	56	70	111

4 THE WALL-SOURCE MODEL

For short or laterally thin targets the cascade generally does not fully develop in the target. Many of the high-energy secondaries can escape from the target and generate their cascades in the shield-walls. The situation is illustrated in Figure 8. In this Wall-Source model, the dose at the point P comes principally from the distribution of secondary sources S′ in the initial layers of the shield-wall, *i.e.* in the case of strongly oblique incidence of the secondaries on the wall, sideways build-up/attenuation dominates over line-of-sight contributions This has been known in shielding studies for low-energy neutrons and photons for some considerable time, however it is not evident that this model should be applicable to high-energy radiation. The secondary source strength is a function of R and θ, depending also on the initial target length and radius as well as the proton energy, but the attenuation in the wall is now a function of d only. The dose at P will be an area integral of the form $\exp(-s/\lambda)/s^2$ where s is the distance of the elemental area of wall source from the point P.

It was shown in [6] that for a thin target in cylindrical geometry the propagation of the cascade in the shield behaved in a similar way to the radiation from a line source situated on the inner surface of the shield where the variation with depth d is given by the Moyer-Integral:

$$D = k\frac{1}{d}\int_0^{\pi} \exp(-\beta\theta)\exp(-d/\lambda\cos\theta)\mathrm{d}\theta \quad (4)$$

In the case of a flat wall it is to be expected that the source will approximate rather to a uniform plane source dis-

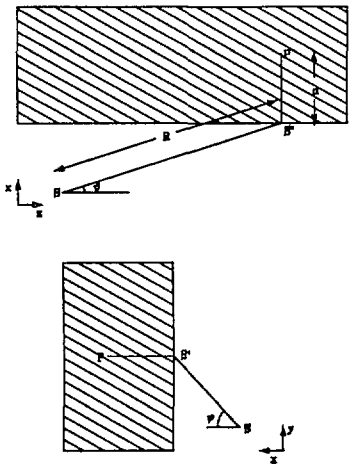

Figure 8: Sketch of geometry used in the wall-source model calculations for an iron cylinder close to a flat shield-wall.

tributed over the surface of the shield wall rather than to a simple line source.

Figure 9 shows the attenuation of plane, line and point isotropic sources through a wall. For simplicity the attenuation length has again been chosen as 50 cm. The inverse square law dependence has been removed in each case by multiplying the dose at the point of interest by the square of the perpendicular shield thickness. The lower curve is for a plane source distributed over the wall surface, the middle curve for a line source and the upper line the simple attenuation for a point source. The curves are normalized to the uniform wall-source attenuation at a depth of 10 metres.

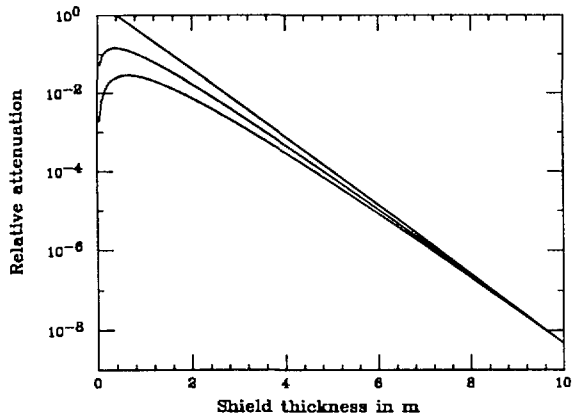

Figure 9: The attenuation of an isotropic source through a flat shield-wall. The upper line is a simple point source, the middle curve corresponds to a line source and the lower curve to a uniform plane source. All curves are normalized at a depth of 10 m.

Figure 9 indicates that at large depths all source types behave as a simple point source. The reason for this is that the negative exponential of distance effectively removes all contributions other than those closest to the source, and at large distances, this small contributing surface resembles a point.

The same data from the FLUKA simulations which were used to test the point-source/line-of-sight model were also used to test the wall-source model. When the value of the dose at a given perpendicular depth in the shield, multiplied by the square of the depth, is plotted as a function of θ and ϕ, where the angles now correspond to the vector linking the source S to S′ instead of linking S to P as in Figure 3, the results shown in Figures 10 and 11 are obtained for the thick and thin radial targets respectively.

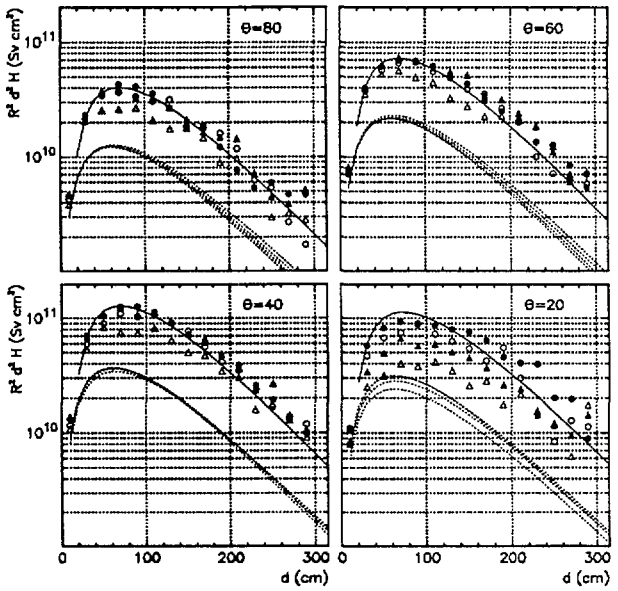

Figure 10: Attenuation perpendicular to the wall for various polar angles, θ, for a 20 cm radial thickness target. Closed circles – $\phi = 0°$, Open circles – $\phi = 15°$, Closed triangles – $\phi = 30°$, Open triangles – $\phi = 45°$. For an explanation of the curves see the text.

The points for all values of ϕ at a given θ scatter around unique curves, apart from effects due to poor statistics. Also shown in these figures are lines calculated using a wall-source model where the source strength required for the surface integral is given by the simulated star-density distribution underneath the point of interest in the first 20 cm bin of the shield. As before a value of 50 cm was used for the effective absorption mean free path. The dashed curves calculated using the wall-source model reproduce well the form of the FLUKA simulations. An almost exact agreement, shown by the solid curves, can be obtained on an absolute basis by normalizing the 20 cm depth point of the model calculations to the 30 cm depth point of the FLUKA simulations. This normalization uncertainty is to be expected since in reality the source for the model calculations is not in fact a surface source but is distributed in depth over the first few tens of centimetres of the shield. However the overall agreement of this simple wall-source model with the data from the FLUKA simulations suggests that, even for the thick radial target case, the dose at a given point is more affected by the radiation coming perpendicularly through the shield than that coming along the line-of-sight from the primary target

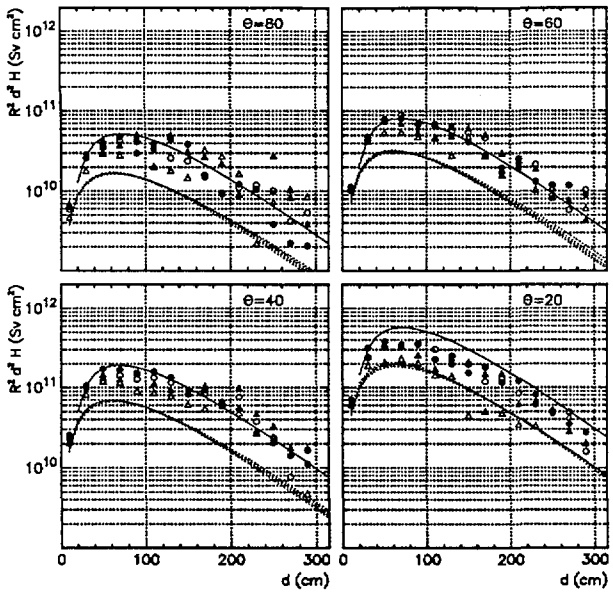

Figure 11: Attenuation perpendicular to the wall for various polar angles, θ, for a 2 cm radial thickness target. Closed circles – $\phi = 0°$, Open circles – $\phi = 15°$, Closed triangles – $\phi = 30°$, Open triangles – $\phi = 45°$. For an explanation of the curves see the text.

to the point of interest.

This conclusion is confirmed by considering the results from a simulation where a "black hole" was inserted in the inner layers of the shield downstream of the proton entry point to absorb the component coming perpendicularly through the wall (see Figure 12). The comparison of the original attenuation taken from Figure 6 for $\theta = 40°$ and the simulation with the black hole in the wall shows that, with the black-hole, the line-of-sight model is again appropriate and one finds the expected value of λ (50 cm).

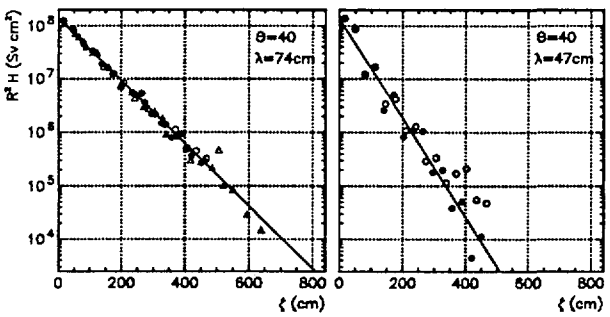

Figure 12: Attenuation along the line of sight for a polar angle $\theta = 40°$, for a 20 cm radial thickness target, without and with a black-hole in the wall. Closed circles – $\phi = 0°$, Open circles – $\phi = 15°$, Closed triangles – $\phi = 30°$, Open triangles – $\phi = 45°$.

5 COMPARISON OF LINE-OF-SIGHT AND WALL-SOURCE MODELS

An attempt was made to predict the form of attenuation found in the point-source/line-of-sight comparisons from the wall-source model in order to investigate further the validity of this latter model. As before, consideration was restricted to the isotropic wall-source and the strength of the source was taken to be the star-distribution in the first layer of the shield, as in the comparisons of Figures 10 and 11. The doses along the appropriate lines-of-sight were calculated from the wall-source model and plotted against the data from the simulations illustrated in Figures 6 and 7. The resulting comparisons are given in Figures 13 and 14.

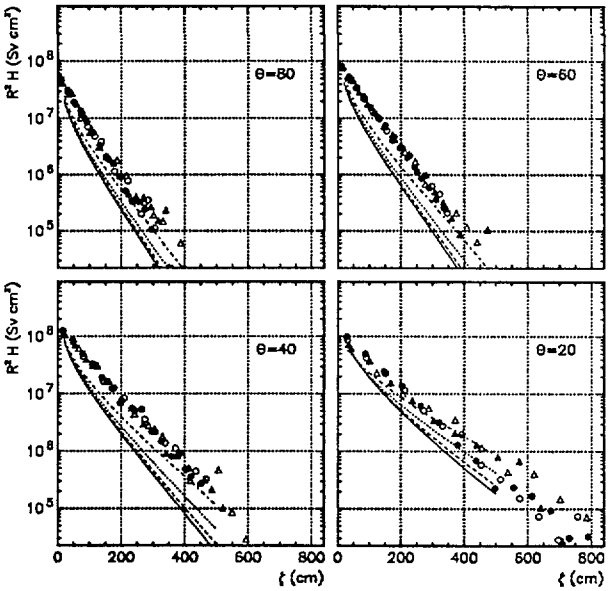

Figure 13: Comparison of attenuation along the line of sight for various polar angles, θ, for a 20 cm radial thickness target as determined from the FLUKA simulations (point data) and as predicted from the wall-source model (lines). Closed circles and solid line – $\phi = 0°$, Open circles and dashed line – $\phi = 15°$, Closed triangles and dotted line– $\phi = 30°$, Open triangles and dashed/dotted line – $\phi = 45°$.

In these Figures no attempt has been made to improve the normalization. The result is that the curves show the same discrepancy of a factor of about three as was found in Figures 10 and 11. However the increase in effective absorption length λ with decreasing polar angle θ is evident and the values of the slope of the attenuation are clearly a good fit to the FLUKA simulations.

This study gives added conviction that the attenuation in the flat shield wall is better represented by a wall-source model for both the radially thick ($r = 20$ cm) and radially thin ($r = 2$ cm) iron targets.

6 CONCLUSIONS

The present study of attenuation of the cascade initiated by a proton beam striking a long magnet system in a flat

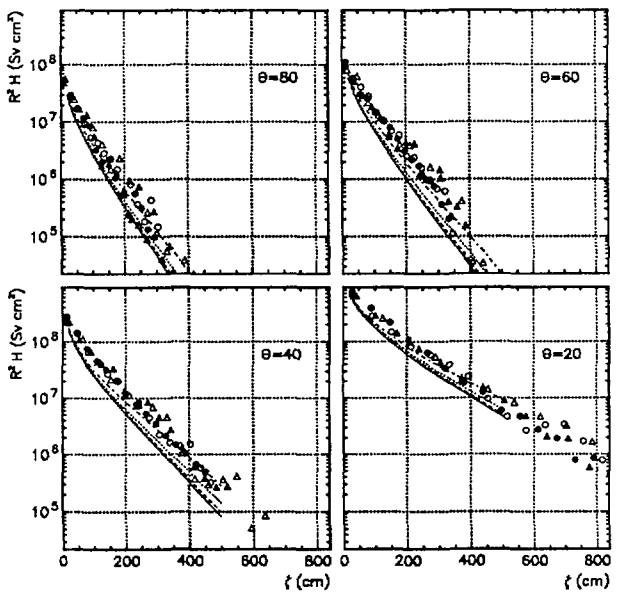

Figure 14: Comparison of attenuation along the line of sight for various polar angles, θ, for a 2 cm radial thickness target as determined from the FLUKA simulations (point data) and as predicted from the wall-source model (lines). Closed circles and solid line – $\phi = 0°$, Open circles and dashed line – $\phi = 15°$, Closed triangles and dotted line– $\phi = 30°$, Open triangles and dashed/dotted line – $\phi = 45°$.

shield wall has shown that the dose contours in the wall are severely affected by the attenuation of the magnets themselves. At very-forward angles, this leads to an increase of dose at the wall surface with increasing vertical distance from the beam axis. As a consequence, detailed magnet structures and realistic shields are *de rigeur* when estimating dose rates in the forward direction, in contrast to the simplifications which can be accepted when estimating lateral doses.

It has been suggested that the transmission of radiation in the shield can be better represented by a wall-source model, where the effective source is the distribution of secondary interactions in the initial layers of the shield wall, rather than by a point-source/line-of-sight model where the point source is concentrated around the initial interaction point of the protons. This is especially interesting since a high-energy property of the cascade (star density) was used to estimate dose equivalent. It has been shown that the wall-source model is capable of predicting the apparent increase in effective mean free path with decreasing angle to the proton beam, found when using the line-of-sight model.

This study indicates that care must be taken in predicting lateral shielding requirements in the very-forward region, especially when the loss of protons occurs in thin or short objects.

7 REFERENCES

[1] A. Fassò, A. Ferrari, J. Ranft and P. R. Sala, "FLUKA: present status and future developments," Proc IV Int. Conf. on Calorimetry in High Energy Physics, La Biodola (Is. d'Elba), Sept. 20–25 1993. Ed. A. Menzione and A. Scribano, World Scientific, p. 493 (1993).

[2] A. Fassò, A. Ferrari, J. Ranft and P. R. Sala, "FLUKA: Performances and Applications in the Intermediate Energy Range," Specialists' Meeting on Shielding Aspects of Accelerators, Targets and Irradiation Facilities. Arlington, Texas, April 28–29, 1994 NEA/OECD document pp 287–304 (1995).

[3] M. Huhtinen and G. R. Stevenson "Geometry Effects on Shielding Requirements for the LHC Main Ring," CERN Internal Report TIS–RP/IR/95–17 (1995).

[4] G. R. Stevenson and M. Huhtinen, "A Lateral Shielding Study for the LHC Main Ring," CERN Internal Report TIS-RP/IR/94-33 (1994).

[5] R. H. Thomas and G. R. Stevenson, "Radiological Safety Aspects of the Operation of Proton Accelerators," Technical Report Series No 283, IAEA Vienna (1988)

[6] A. Fassò, K. Goebel, M. Höfert, J. Ranft et G. R. Stevenson, "Shielding against high-energy radiation," Landolt-Börnstein, Numerical data and Functional Relationships in Science and Technology, New Series, Group I: Nuclear and Particle Physics, Volume 11, Springer-Verlag [Berlin] (1990).